Journal of Sol-Gel Science and Technology (2022) 101:244–255
https://doi.org/10.1007/s10971-021-05681-0

ORIGINAL PAPER: SOL-GEL AND HYBRID MATERIALS FOR BIOLOGICAL AND HEALTH (MEDICAL) APPLICATIONS

Modified zinc oxide nanoparticles against multiresistant *Enterobacteriaceae*: stability, growth studies, and antibacterial activity

Bruna Lallo da Silva[1] · Mariana Marin Garcia[2] · João Augusto Oshiro-Junior[3,4] · Mariana Rillo Sato[1] · Bruno Leonardo Caetano[1,4,5] · Leila Aparecida Chiavacci[1]

Received: 9 September 2021 / Accepted: 29 October 2021 / Published online: 9 January 2022

Abstract

The development of new strategies to combat bacterial growth is a focus of many studies. Zinc oxide nanoparticles (ZnO NP) have been shown to possess great antibacterial activity. ZnO NP antibacterial activity is highly dependent on particle size, with smaller sized NP achieving higher performance. Based on this property, in the current study, we have demonstrated the formation and growth of small ZnO NP with 5 nm synthesized by a sol–gel method and characterized by small-angle X-ray scattering (SAXS). The radius of the ZnO NP increased throughout the synthesis, being more pronounced in the beginning of the synthesis (10–20 min) and continuing to grow more slowly until 180 min. The surface of the ZnO NP was modified by (3-glycidyloxypropyl) trimethoxysilane (GPTMS) dispersed in water without significant changes to the ZnO NP size. GPTMS-ZnO NP stability studies realized by zeta potential, SAXS, and UV–vis spectroscopy demonstrated that GPTMS-ZnO NP dispersed in water were stable for 62 days when stored at 5 °C and for 35 days when stored at room temperature, with no size increase detected. ZnO NP dissolve in acidic pH, are stable at alkaline pH, and form fractal aggregates at pH 7. The GPTMS-ZnO NP antibacterial activity against ESBL-producing *Escherichia coli* and carbapenemase (KPC)-producing *Klebsiella pneumoniae* was assessed. The GPTMS-ZnO NP had excellent antibacterial activity. To date, there are no studies on GPTMS-ZnO NP antibacterial activity against multiresistant *Enterobacteriaceae*. Thus, this study indicates that GPTMS-ZnO NP have great potential to combat multiresistant enterobacteria.

Graphical Abstract

Grow and stability studies of zinc oxide nanoparticles. The radius of ZnO NP increased more pronouncedly in the beginning of the synthesis. The GPTMS-ZnO NP had high size stability. GPTMS-ZnO NP have great potential to combat multiresistant *Enterobacteria*.

✉ Leila Aparecida Chiavacci
leila.chiavacci@unesp.br

[1] School of Pharmaceutical Sciences, Department of Drugs and Medicines, Highway Araraquara-Jaú, São Paulo State University (UNESP), Araraquara, SP, Brazil

[2] Graduation Program in Pharmaceutical Sciences, State University of Paraíba, Av. Baraúnas, 351, Campina Grande, PB 58109-753, Brazil

[3] UNIFACISA Centro Universitário, Campina Grande, PB, Brazil

[4] Soft Matter Sciences and Engineering, ESPCI Paris, PSL University, Sorbonne Université, CNRS, F-75005 Paris, France

[5] Physico-chimie des Electrolytes et Nanosystèmes Interfaciaux, PHENIX, Sorbonne Université, CNRS, F-75005 Paris, France

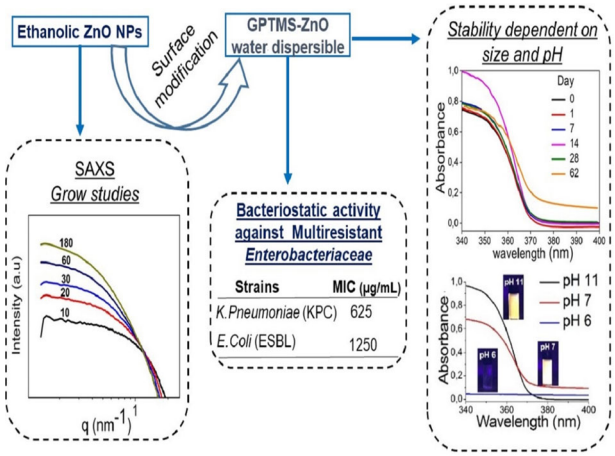

Keywords Bacterial resistance · Zinc oxide nanoparticles · Surface modifier · Stability · Size

Highlights

- ZnO nanoparticles increased more pronounced in the synthesis beginning and continues to grow more slowly until 180 min.
- ZnO nanoparticles modified with GPTMS were stable in water for at least two months with no size increase.
- ZnO nanoparticles are stable at alkaline pH, origins fractal aggregates at pH 7 and dissolves at acid pH.
- ZnO nanoparticles had excellent antibacterial activity against Multiresistant *Enterobacteriaceae.*

1 Introduction

The inappropriate use of antimicrobials leads to the selection of multiresistant strains. The World Health Organization (WHO) estimates that, by 2050, infections by resistant microorganisms could cause 10 million deaths per year worldwide and become an important public health problem [1, 2]. Among the species that are multiresistant, *Enterobacteriaceae* has gained attention because it has numerous genera and species, with a complex structure that produces toxins, including resistance genes and other virulence factors. Some species are part of the human microbiota, but sometimes can cause disease. Commonly, the most clinically isolated bacteria are strains of *Escherichia coli*, *Klebsiella pneumoniae*, and *Enterobacter aerogenes* [3].

The advanced resistance mediated by beta-lactamases impairs the treatment of these infections, since they are treated mainly by beta-lactam antibiotics, such as cephalosporins and carbapenems [4]. The extended-spectrum beta-lactamases (ESBL) mediate resistance to third generation cephalosporins and penicillin and are presented worldwide in the *Enterobacteriaceae* species [5]. carbapenemase (KPC), which are beta-lactamases capable of hydrolyzing carbapenems and inactivating the classes of fourth-generation cephalosporins, are routinely found in hospital and health establishments [3, 6, 7]. Thus, one of the main research challenges is to develop antibacterial drugs that are able to combat these multidrug-resistant strains, including the *Enterobacteriaceae*, such as ESBL-producing *Escherichia coli* (ESBL-*E.coli*) and KPC-producing *Klebsiella pneumoniae* (KPC-*K.pneumoniae*)

Based on this problem, new strategies have been studied to overcome the areas in which antibiotic actions fail. Advances in the nanotechnology field enable the development of nanoparticles with different sizes, morphology, and shapes, which allow for interactions between the nanoparticles and bacterial cells and the development of new biocidal agents. Compared to organic NP, inorganic NP have many advantages, such as better stability, greater durability, less toxicity to the user, less microbial resistance, and good selectivity [8].

Among all inorganic materials, ZnO NP have attracted attention due to their highest photocatalytic efficiency and greater biocompatibility. Additionally, ZnO NP have greater selectivity and better durability and heat resistance, and have been studied extensively for their antibacterial activity. [8–14]. The ZnO NP antibacterial activity involves the production of reactive oxygen species (ROS), Zn^{2+} liberation, and disruptions in the bacterial cell membrane. Since ZnO NP act in a non-specific way, [15, 16], this

makes them promising alternatives for combating multidrug-resistant bacteria because it acts in different pathways of antimicrobial organic drugs. In this way, the main mechanisms of antibiotic resistance are almost irrelevant. Besides, the mechanisms do not require, necessarily, the ZnO NP to be internalized by the cell. For all these reasons, the use of ZnO NP result in a low probability of bacterial resistance [9].

ZnO NP can be obtained by several synthesis routes. Among all of them, the sol–gel method has advantages because it produces small nanoparticles, it is a practical and economical approach, and it is easily transferred to large-scale production [8, 17, 18]. However, there is a crucial point: the ZnO NP produced by the sol–gel route are unstable in water, leading to aggregation and increased size. To overcome this limitation, researchers have used an organosilanes surface modifier because they covalently bind to the hydroxylated surface of ZnO NP, creating a protection barrier that allows for the dispersion of the NP in an aqueous medium [8, 19, 20].

The antimicrobial activity of ZnO NP can be improved when the size is decreased [8, 10]. Thus, knowing the formation and growth mechanisms of ZnO NP, as well as maintaining the nanoparticle size after their synthesis, are very important to provide optimized antibacterial activity.

Here, we report studies on the formation and growth of ZnO NP and stability studies about their size after surface modification with (3-glycidyloxypropyl) trimethoxysilane (GPTMS). We evaluate the antibacterial activity of 5 nm diameter GPTMS-ZnO NP against multiresistant ESBL-*E. coli* and KPC- *K. pneumoniae*. The nanoparticles are very small, and studies about GPTMS-ZnO NP against these strains cannot be found in the literature, which makes our research highly innovative and relevant.

2 Materials and methods

2.1 Materials

Zinc acetate dihydrate, (Qhemis-Brazil); lithium hydroxide monohydrate (Vetec-Brazil); absolute ethanol (Synth-Brazil); (3-Glycidyloxypropyl) trimethoxysilane,(GPTMS) (Sigma-USA); Muller Hilton broth (HIMEDIA-India); Resazurin (Sigma-USA); Muller Hilton Agar (HIMEDIA-India).

2.2 ZnO NP synthesis

2.2.1 Precursor

The $Zn_4O(Ac)_6$ tetrameric precursor was prepared through refluxing of an ethanolic solution containing 0.05 M zinc acetate at 80 °C for 2 h. At the end of the reaction, the transparent precursor was stored at −10 °C.

2.2.2 Ethanolic ZnO NP colloidal suspensions

The ZnO NP were prepared by a sol–gel method proposed by Spanhel and Anderson with some modifications [18]. ZnO NP were obtained by the hydrolysis and condensation reactions through the addition of LiOH in different hydrolysis ratios, $r = ([OH^-] / [Zn^{2+}])$ in a $Zn_4O(Ac)_6$ precursor. The reaction was conducted at 50 °C under an ultrasound bath for 3 h (GPTMS-ZnO-3h). For the GPTMS-ZnO-24h sample, the reaction was conducted at an ultrasound bath at 50 °C, followed by 21 h of magnetic stirring at 50 °C This process produced the GPTMS-ZnO-3h and GPTMS-ZnO-24h ethanolic ZnO NP colloidal suspensions that were stored at −10 °C to maintain colloidal stability.

2.2.3 Surface modified ZnO NP

The ZnO NP with a modified surface were obtained by adding 0.1 M GPTMS and 0.2 M LiOH to 10 mL of the ethanolic ZnO NP colloidal suspension. The reactions were performed in an ultrasound bath for 30 min at room temperature for both samples, GPTMS-ZnO-3h and GPTMS-ZnO-24h ethanolic ZnO colloidal suspensions. This resulted in the formation of a white precipitate, which was separated by centrifugation (4000 rpm, 10 min) and vacuum dried at room temperature. This process produced the GPTMS-ZnO-3h and GPTMS-ZnO-24h powders that were then dispersed in Milli-Q water at 5 mg/ml and stored at 4 °C to maintain colloidal stability.

2.3 Characterization techniques

2.3.1 Small angle X-ray scattering (SAXS)

The SAXS curves for ZnO NP with and without a surface modifier were obtained at the SAXS-1 beamline at the Brazilian synchrotron source-LNLS (Campinas, Brazil). The SAXS analyses were carried out at a line containing a monochromator ($\lambda = 1.488$ Å), a vertical detector located about 0.9 m from the sample, and a multichannel analyzer to record the scattering intensity, I(q), as a function of the scattering vector, q. Data analyses were performed using the software package SASFIT [21]. It is important to highlight that the SAXS data were normalized according to the acquisition and transmission time of each sample, and the dispersed intensity of the sample holder and the solvents used (ethanol and water) were subtracted from the total intensity. For ZnO NP growth studies, the precursor was previously prepared following the processes described in section 2.2.1. An ethanolic LiOH solution was prepared

at 0.1 M. Both the LiOH solution and the precursor were placed in a capillary in a volume necessary to result in $r = [OH^-] / [Zn^{2+}] = 1.0$. Later, this capillary was added to the Linkan oven, which allowed for the temperature to be controlled at 50 °C for 180 min.

2.3.2 Zeta potential

The zeta potential of the ZnO NP dispersions in water at 5 mg/mL was measured with a ZetaSizer Nano ZS Zen3600 (Malvern Instruments) using acid-base titration. The measurements were made in triplicate and the pH was adjusted with solutions of HCl (0.1 M) and NaOH (0.1 M), within the pH range 3–11.

2.3.3 UV–vis spectroscopy (UV–vis)

The absorption spectra of ZnO NP dispersed in water were collected using a Cary Win 4000 UV–vis spectrophotometer. The UV–vis spectra were corrected from the absorption spectrum of water. The spectra were obtained between 340 and 400 nm, with a wavelength step of 1 nm, using an immersion probe with a 2 mm optical path and an average counting time of 0.2 s per point. To access data on stability, the ZnO NP dispersed in water were stored at room temperature for 62 days and at 5 °C for the maximum period in which the ZnO NP excitonic peak was found.

2.4 Antibacterial activity

The determination of the minimum inhibitory concentration (MIC) of ZnO NP was performed against strains of enterobacteria with different sensitivity profiles. For this, we used a strain of *Escherichia coli* ATCC 25922 and clinical strains from the collection of a private laboratory network of Campina Grande with known sensitivity profiles, such as ESBL-producing *Escherichia coli* and KPC-producing *Klebsiella pneumoniae*. To determine the MIC, the broth microdilution technique was used, as described by the Clinical Laboratory and Standards Institute M07-A10 [22]. To perform the test, the inoculum was standardized in a spectrophotometer at a wavelength of 625 nm to obtain the correct optical density of turbidity control, which must vary from 0.08 to 0.10 to obtain the standard McFarland solution of 0.5, resulting in a suspension containing approximately 1 to 2×10^8 CFU mL^{-1}. To obtain a final concentration of 5×10^6 CFU mL^{-1}, a dilution of 1:20 was performed in the suspension that was obtained.

One hundred microliters of ZnO NP dispersed in water were added to the microplate wells containing 80 µL of the Mueller Hinton broth and 20 µL of the adjusted inoculum, resulting in a final concentration of 5×10^5 CFU mL^{-1}. The plates were incubated at 35 ± 2 °C for 20 h. The MIC was defined as the lowest concentration that inhibited visible microbial growth, confirmed after the addition of 20 µL of resazurin in each well of the plate. The analyses were performed in triplicate. In parallel, the viability of the strain (growth control) and the sterility control of the medium was performed. From the results obtained by the MIC, the minimum bactericidal concentration (MBC) was determined. With the aid of the platinum loop, 1 µL was removed from the well and seeded in Petri dishes with Mueller Hinton agar. The plates were incubated at 35 ± 2 °C for 24 h. After this, it was possible to observe whether there was bacterial growth.

3 Results and discussion

3.1 SAXS studies

The ZnO NP sizes can directly influence their antibacterial activity [8, 10]. For this reason, the SAXS technique was chosen to study the influence of the size dependence on two synthesis parameters: the hydrolysis ratio and reaction time, which can influence the size of the nanoparticles synthesized by the sol–gel route [18, 23, 24].

Figure 1 shows the SAXS curves in a log:log plot of the scattering intensity I (q) versus the scattering vector (q) of ZnO NP with different hydrolysis ratios $r = 1.0$, 1.4 dispersed in water. The SAXS profiles for samples of $r = 1.0$ and 1.4 were relatively similar. The plateau observed in low q values correspond to the Guinier region, characteristic of the scattering of a diluted particle system [25].

Through the SAXS curves, which presented the plateau at lower q values, it was possible to apply a mathematical

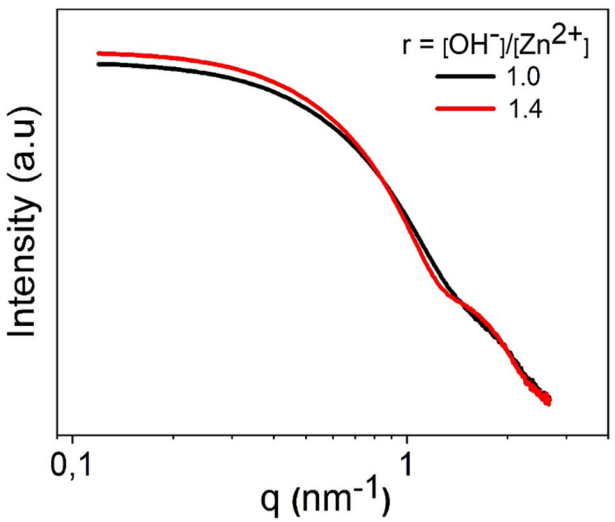

Fig. 1 SAXS curves of ZnO NP synthesized with different hydrolysis rations $r = [OH^-] / [Zn^{2+}] = 1.0$ and 1.4. These ZnO NP were modified using GPTMS and dispersed in water

Table 1 Time and storage dependent UV–Vis radius of GPTMS-ZnO NP, calculated by the Brus equation

Samples	Storage temperature (°C)	Storage time (days)	Radius (nm)
GPTMS-ZnO-3h	5	0	3.1
		62	4.1
	room temperature	0	3.1
		14	3.3
GPTMS-ZnO-24h	5	0	4.0
		62	5.3
	room temperature	0	4.0
		35	4.5

model to calculate the radius of gyration (Rg) that corresponds to the radius of the particles or aggregates, which can be calculated according to Eq. (1). The SAXS curves were also adjusted by a homogeneous sphere shape factor using LogNor radius distribution. In this way, the radius of the sphere (R sphere) was obtained. The Rg of the ZnO NP synthesized with a hydrolysis ratio of 1.0 and 1.4 were 5.2 and 3.7, respectively, and Rsphere of the ZnO NP synthesized with a hydrolysis ratio of 1.0 and 1.4 were 4.7 and 3.5, respectively (support information, Fig. 1, and Table 1).

$$I(q) = I(0)^{\left(-Rg^2\frac{q^2}{3}\right)} \quad (1)$$

where *I (0)* is the scattering intensity given by the relation between the electron density given between the phases *(p0-pm)*, number *(N)*, and mean volume *(V_0)* of the particles, as shown in Eq. (2).

$$I(0) = N(p0 - pm)^2 V_0^2 \quad (2)$$

ZnO NP obtained with hydrolysis ratio 1.4 resulted in a turbid dispersion and ZnO NP synthesized with hydrolysis ratio 1.0 resulted in a translucid dispersion. Do Kim et al. statically showed that the optimal size control of ZnO NP produced by the sol–gel route was obtained with the hydrolysis ratio of 1.0. In this way, we choose this parameter for next experiments [26]. Because the time reaction can influence the ZnO NP size, we changed this parameter, as reported in our previous study. GPTMS-ZnO-3h had a Rg of 5.2 nm and Rsphere of 4.7 nm, while GPTMS-ZnO-24h had a Rg of 5.5 and Rsphere of 4.5 [8].

It is important to highlight that the SAXS curve profiles of ZnO NP synthesized in 3 and 24 h with $r = 1.0$ were very similar, with no significant differences in relation to the sizes of the nanoparticles formed. Thus, the reaction monitoring was carried out for 3 h, following the procedure previously described in the methodology (section 2.3.1). In addition, it is important to note that the analyzed ZnO NP are without GPTMS, since the surface modification is a step performed after the ZnO NP synthesis.

Figure 2A shows the SAXS curve evolution of the ZnO NP time dependence (180 min). To better illustrate this, some curves have been selected and are shown in Fig. 2B. The curves show characteristics of diluted particle systems; thus, at low values of q, there is the presence of a plateau corresponding to the Guinier region where the scattering intensity can be accompanied by Eqs. (1) and (2). There is a change in the curve patterns according to the reaction time. The Guinier region displace to smaller q values according to an increase in the reaction time, showing an increase in the ZnO NP sizes that are formed.

Figure 3 shows the time evolution of I(0) and Rg. An increase in I(0) is observed throughout the reaction. I(0) is related to the number and nanoparticle size, as shown in Eqs. (1) and (2). The Rg increased throughout the synthesis, indicating that the individual nanoparticles increase in size or aggregate, forming larger structures. This increase was more pronounced in the 10 to 20 min of the reaction time, going from 1.50 nm to 2.55 nm. After that, the ZnO NP continue to grow more slowly. For example, in 120 min, the Rg was 3.9 nm, while in 180 min, it was 4.1 nm.

During all the reaction time, I(0) of the SAXS curves increases and the same profile was obtained with the Rg. This result indicates that the number of ZnO NP increases as the nucleation process occurs. However, probably, the equilibrium between ZnO NP and precursor species is not established, which favors the formation and growth of new ZnO NP [27].

Caetano et al. studied the formation, growth, and aggregation of ZnO quantum dots. The results showed that first, the nucleation and growth of the ZnO particles occurred, which was triggered by the consumption of zinc oxyacetate precursor. In an intermediate stage, there was the compact growth of aggregates and the primary particles coalesce. The next stage showed growth of the fractal aggregates and finally, there was a second stage of nucleation and growth of the fractal aggregates, which demonstrate that after the nucleation step, the particles can continue to grow through a coalescence or aggregation process [27].

The SAXS results allowed us to select the hydrolysis ratio to continue the studies, in addition to providing information on the formation mechanisms and growth of ZnO NP synthesized by the sol–gel method, which allow us to monitor the stages of formation and growth of the nanoparticles [27, 28]. Exploring the mechanisms by which the ZnO NP increase in size is relevant since, in a previous study, it was shown that size directly influences antibacterial activity. Smaller ZnO NP (less than 10 nm) had better antibacterial activity than 30 nm ZnO NP [8].

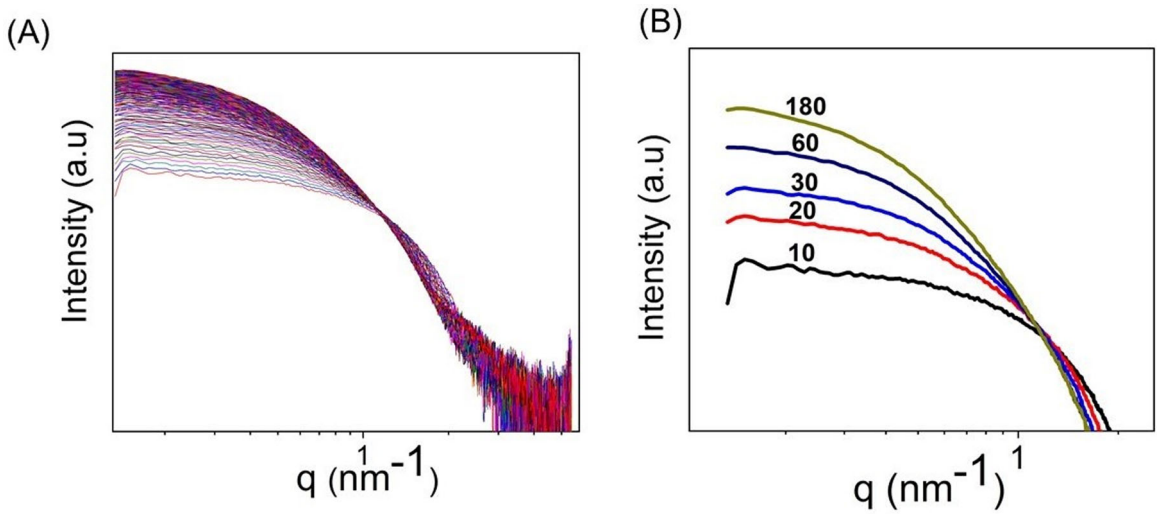

Fig. 2 **A** SAXS curves evolution recorded in situ during the formation of ZnO NP and (**B**) selected in situ SAXS profiles measured at the indicated reaction time (min)

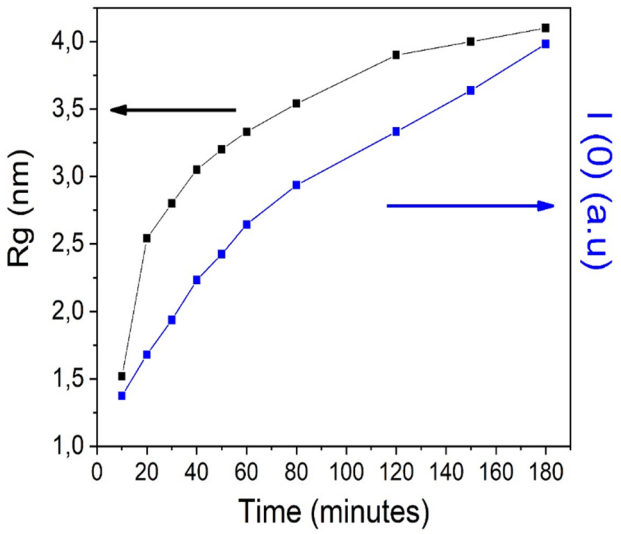

Fig. 3 Time evolution of I(0) and Rg for ZnO NP

In summary, the hydrolysis ratio directly influences the size of the nanoparticles formed. In addition, the size of the ZnO NP increases as the reaction time increases for a period of 180 min; however, the growth is more pronounced in the first minutes of the reaction. The increase in the Rg follows the increase in I(0), indicating that new particles are formed during the entire reaction time of 180 min, probably because there is no equilibrium between the precursor species and the ZnO NP.

3.2 Stability studies

Although the SAXS technique is accurate for assessing nanoparticle size, the absorption spectrum in the UV–vis region is simpler to assess stability over a period of months. It is also possible to evaluate ZnO NP size by UV–vis. Thus, the size evolution during the long-term stability studies of ZnO NP can be determined from the absorption spectra in the UV–vis region using the effective mass model derived by Brus [29] (Eq. (3)). Through the method proposed by Nidelijkovi [30], the wavelength limit (λ_c) was determined by the intersection of the tangent to the excitonic peak up to the wavelength threshold. From λ_c, it was possible to calculate the average size of NP since the limit wavelength is related to the band gap (Eg = hc / λc), where h is the Planck´s constant and c is the speed of light. Finding the Eg value was possible to obtain the nanoparticle radius. Thus, we used the UV–vis spectra to evaluate the stability of ZnO NP modified with GPTMS and dispersed in water through the displacement of the ZnO NP excitonic peak.

$$E_{g(QD)} = E_{bulk} + \frac{h^2}{8R^2}\left(\frac{1}{m_e^*} + \frac{1}{m_h^*}\right) - \frac{1.786e^2}{4\pi\varepsilon_0\varepsilon_r R^2} \quad (3)$$

E_g = band gap energy of quantum dot; E_{bulk} = band gap energy of bulk semiconductor ($E_{bulk} = 3.4$ eV); h = Planck's constant (6.62×10^{-34} J·s); m_e^* = effective mass of excited electron ($m_e^* = 0.24$); m_h^* = effective mass of excited hole ($m_h^* = 0.45$); ε_0 = permittivity of vacuum (8.854×10^{-14} F); ε_r = relative permittivity (3,7) and R = quantum dot radius

Figure 4 shows the stability study of the GPTMS-ZnO-3h sample. It was possible to observe that after 28 days of storage at 5 °C (Fig. 4A), the UV–vis absorption spectra shifted to greater wavelengths; however, the displacement was not very significant. In addition, longer storage times decreased absorbance. For storage at room temperature

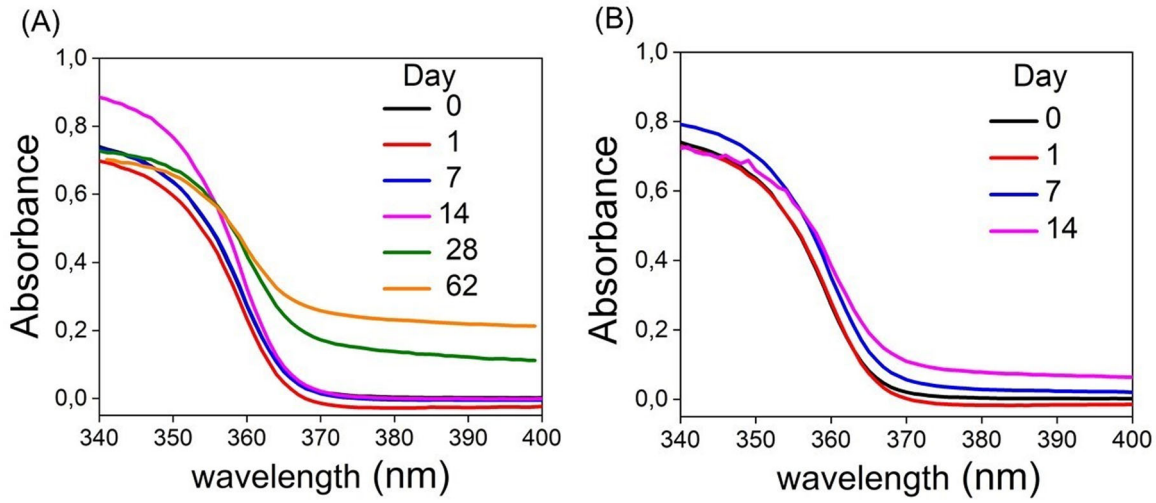

Fig. 4 UV–Vis absorption spectra of GPTM-ZnO-3h, dispersed in water, stored at 5 °C (**A**) and at room temperature (**B**)

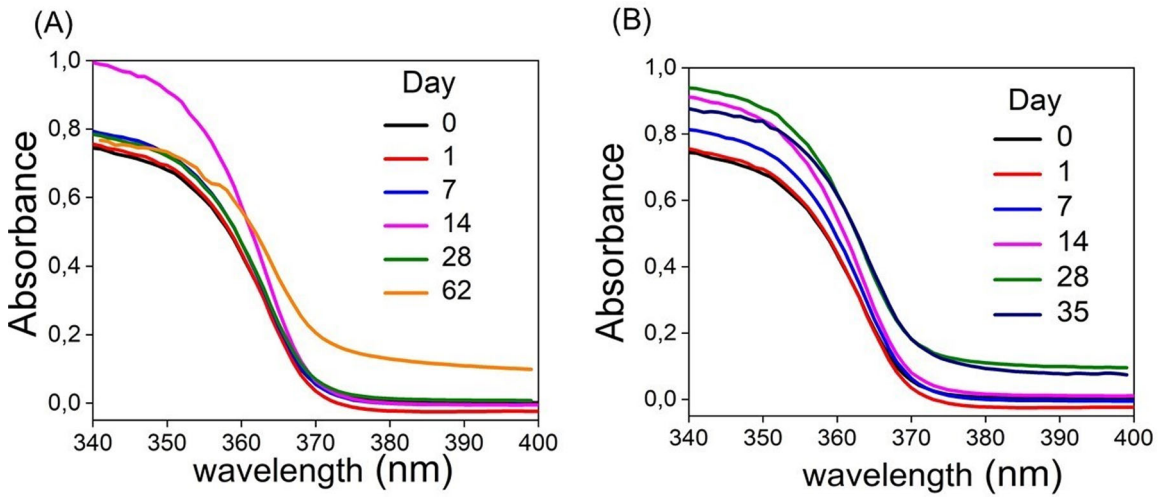

Fig. 5 UV–Vis absorption spectra of GPTM-ZnO-24h, dispersed in water, stored at 5 °C (**A**) and at room temperature (**B**)

(Fig. 4B), the ZnO NP excitonic peak was detectable for up to 14 days but after this period, the nanoparticle dispersions, which were previously transparent, gave rise to white precipitates. In addition, there was a loss of nanoparticle luminescence.

Figure 5 shows the stability study of the GPTMS-ZnO-24h sample. For storage at 5 °C (Fig. 5A), the ZnO excitonic peak was observed for 62 days. For 28 days, there was no wavelength shift, showing that the ZnO NP remained stable. However, after 62 days, there was a small decrease in absorbance, followed by the presence of noise and a small shift to higher wavelengths. At room temperature (Fig. 5B), it was possible to observe the ZnO excitonic peak up to 35 days of storage and after that period, a white precipitate formed and was followed by a loss of ZnO NP luminescence.

The ZnO NP colloidal ethanolic suspensions are stable for at least two months. These results are not showed. After the surface modification with GPTMS, we demonstrated that precipitates are formed with luminescence loss. Some hypothesis could explain the precipitates formed for both samples and the luminescence loss when storage at room temperature: i) other species are formed such as $Zn(OH)_2$ and/or ii) ZnO NP aggregation, increasing in size and lost the luminescence. The ZnO NP synthesized in this work are quantum dots. In the quantum confinement, the particles have all the three dimensions confined in the 1–10 nm scale and there is the emission of a photon with a wavelength determined by the dimensions of the nanoparticles [31, 32]. Thus, size is highly related to photoluminescent properties and if ZnO NP increase in size higher that 1–10 nm in all the three emissions, there are the luminescence loss.

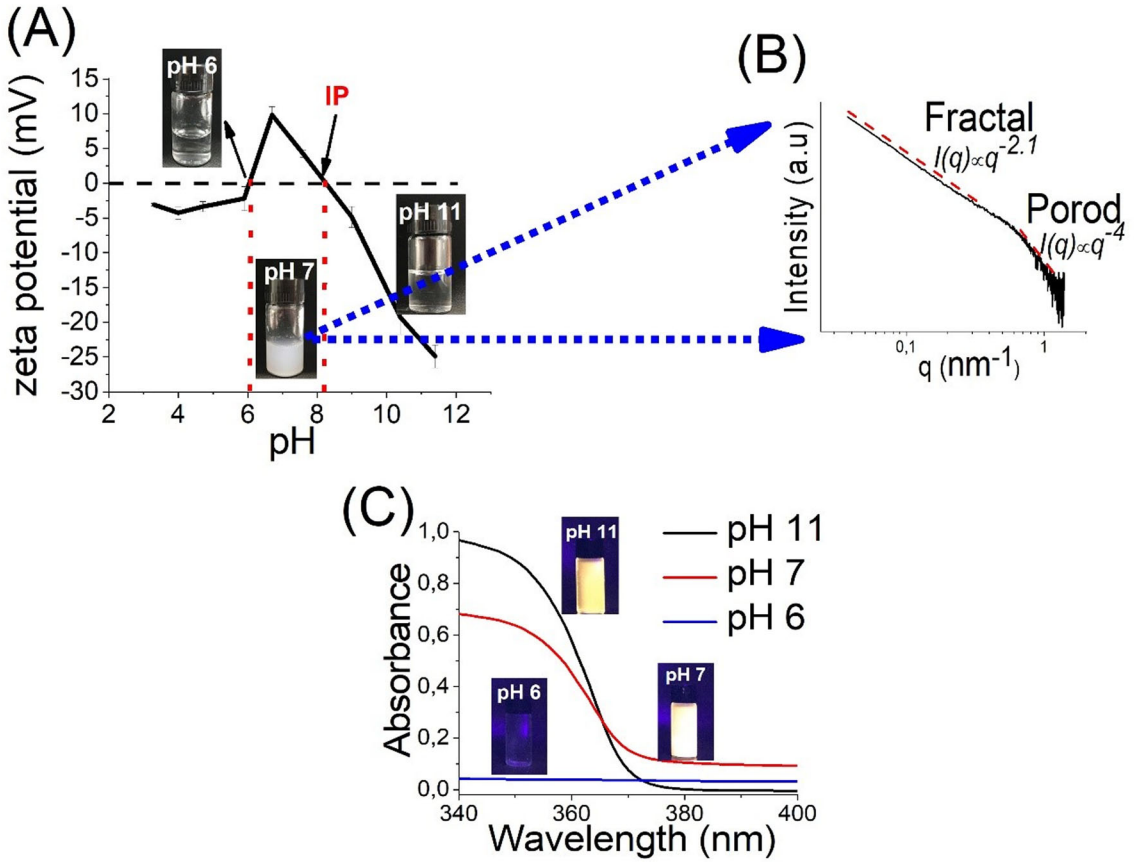

Fig. 6 **A** Zeta potential according to pH changes. **B** SAXS curves of GPTMS-ZnO NP dispersed in water at pH 7 and **C** UV–vis spectroscopy of GPTMS-ZnO NP dispersed in water at different pH values, and images under UV excitation ($\lambda_{exc} = 365$ nm)

However, it is important to highlight that our goal with the stability tests was evaluete the stock conditions to ensure that the samples that were used for antibacterial activity were ZnO NP with small size.

The temperature directly influences the stability of the modified ZnO NP. For GPTMS-ZnO-3h, the stability time was reduced by approximately four times when stored at room temperature (62 days at 5 °C and 14 days at room temperature). As for the ZnO-GPTMS-24h sample, the time at which it remained stable at room temperature was about twice smaller in relation to storage at 5 °C (62 days at 5 °C and 35 days at room temperature).

We applied Eq. (3) to determine the ZnO NP radius for the sample stored at different times and temperatures, as shown in Table 1. The ZnO NP modified with GPTMS and dispersed in water had excellent stability when stored at 5 °C, and could be used for two months without significant changes in the nanoparticle size. Besides, when stored at room temperature, ZnO NP remained stable for 14 days (GPTMS-ZnO-3h), which was extended to 35 days when we increased the sol–gel synthesis time (GPTMS-ZnO-24h). It is worth mentioning that for the ZnO NP modified with GPTMS and stored at 5 °C and at room temperature, for a period of 14 days, there were no significant wavelength shifts, i.e, the size remained almost unchanged. This result corroborates with those presented by Rissi et al. [19], who evaluated the stability of ZnO NP stored at 5 °C, and can be explained by the ability of surface modifiers to protect ZnO NP and decrease their aggregation [8, 33, 34].

We selected the ZnO NP synthesized in 24 h to proceed with the studies for two main reasons. The first is because it had a stability greater than that of the 3 h sample. A hypothesis for the improvement in the stability when ZnO NP were synthesized in 24 h is that in 3 h, we observed no equilibrium between the precursor species and the ZnO NP because the ZnO NP continued to grow as new particles were formed (Fig. 3). This precursor species can cause instability. However, when higher reaction times were used, the precursor species can be consumed, resulting in higher stability. In addition, in our previous study, it was demonstrated that GPTMS-ZnO-24h had better antibacterial activity, with lower MIC values for *S. aureus* and *E. coli* compared to GPTMS-ZnO-3h [8].

Figure 6A shows that the zeta potential value found for pH 11 was approximately – 25 mV. When the ZnO NP are modified with GPTMS, the dispersion in water has a pH of

Table 2 MIC and MBC of GPTMS-ZnO NP against strains of *E. coli* ATCC (25922); ESBL- producing *E. coli* and KPC -producing *K. pneumoniae*

Strains	MIC (μg/mL)	MBC (μg/mL)
E. coli ATCC	625	2500
ESBL- *E. coli*	625	2500
KPC - *K. pneumoniae*	1250	2500

approximately 11. Visually, the sample is transparent, suggesting that the nanoparticles are well dispersed. Thus, the route used for the surface modification resulted in GPTMS-ZnO NP being stable at alkaline pH. However, as the pH decreases, there is an increase in the zeta potential and the isoelectric point (IP) is reached at pH 8.3. This is due to the increase in the attraction forces. Thus, near the IP, the agglomeration of the NP tends to increase [35].

For pH smaller than that found at the IP, the zeta potential starts to be positive (+10 mV). For the colloidal suspension with pH values close to that of the isoelectric point, it was possible to view the formation of aggregates [35, 36]. Figure 6B shows that the SAXS curves at pH 7 are characteristic of an aggregate particle system. At small q values, we did not observe the plateau corresponding to the Guinier region. On the other hand, at small q values, a linear decay occurs ($I(q) \propto q^{-\alpha}$, in which the value of α was −2.1) that result in the formation of fractal aggregates with fractal dimensions characteristic of structures formed by cluster-cluster aggregation that is limited by the reaction [37]. For high values of q, it is possible to observe a second linear regime that obeys the Porod law, with a linear decay of -4 indicating the formation of NP with smooth and well defined surfaces [27].

When pH is close to 6, the zeta potential decreases again, reaching a zero value. It is important to note that, for the nanoparticle dispersion at pH 6, the dispersion becomes transparent again (Fig. 6A. This second point, at which the zeta potential was zero, can correspond to the instability of ZnO NP at acidic pH values as a result of their dissolution [38, 39]. Figure 6C shows the UV–vis absorption spectra of the GPTMS-ZnO NP dispersed in water at different pH values, and the images after excitation at 365 nm with a UV lamp. It is possible to observe the excitonic peak characteristic of ZnO NP and their luminescence at pH 11 and pH 7. However, at pH 6, the excitonic peak of ZnO disappears, and there is loss of luminescence, confirming that ZnO NP dissolve under acidic pH conditions.

3.3 Antibacterial activity

GPTMS-ZnO NP were tested against a standard strain of *E. coli* and isolated clinical samples of multiresistant enterobacteria ESBL-*E.coli* and KPC- *K.pneumoniae* by a microdilution method. The results are summarized in Table 2. The results show that the GPTMS-ZnO NP have the same MIC for *E. coli* ATCC and ESBL- *E. coli*. The same profile was obtained for the MBC. However, for the *K. pneumoniae*, the MIC was obtained at a higher concentration of 1250 μg/mL. For all tested bacteria, the bactericidal activity was observed at 2500 μg/mL (i.e., at a higher ZnO NP concentration).

The exact mechanism of ZnO NP antibacterial activity remains unknown. However, it occurs in a non-specific way by one or more mechanisms: i) reactive oxygen species (ROS), such as hydroxyl anion superoxide (O_2-), hydroxyl radicals (HO_2-), and peroxide hydrogen (H_2O_2), ii) release of Zn^{2+} zinc and internalization of ZnO NP, causing the destruction of cellular components, damaging the metabolic system of amino acids, and ultimately leading to the cellular envelope being damaged and/or ruptured [8, 15, 40].

Organosilanes are precursors of organosilanols or organosilsesquioxanes. They can be used as surface modifiers due to its link with oxides by silyation thought a rapid covalent bond formation [41]. Therefore, some researchers have modified ZnO NP surface with organosilanes, making them stable in water. A study conducted by Rissi et al. have showed that ZnO NP modified with GPTMS formed capping layers interacting by covalent Zn–O–Si bonds with the ZnO surface [19]. The surface modification can be used to improve the ZnO NP stability [8]. However, it is important to highlight that the surface properties of nanomaterials can change the interaction with the cell and thus, increase or decrease the antibacterial activity [42].

The surface modification performed in our study using GPTMS not enhanced its antibacterial activity as showed in a previously work published by our group. Contrary, ZnO NP without surface modification had a smaller MIC values against *S. aureus* and *E.coli*. Even with the small decrease in the antibacterial activity, the surface modification using GPTMS resulted in the interaction with *S. aureus* cells, causing disruption in its cell wall [8]. We have used the same route in this present study. On the other hand, recently Busila et al. have showed that as higher concentration of GPTMS used higher was the antibacterial activity of ZnO NP. However, the researchers attribute the increase in antibacterial activity due to the decrease of nanoparticles size with the use of higher amount of GPTMS [43]. Besides, Farouk et al. showed that the GPTMS molecule did not had an antibacterial activity [44]. Therefore, the most important parameter achieved using GPTMS is maintaining the ZnO NP size because smaller nanoparticles have better antibacterial activity.

Our results show that ZnO NP have excellent antibacterial activity against ESBL-*E.coli*. Hameed et al. [15] studied the antibacterial activity of ZnO NP undoped and doped with neodymium (Nd) against ESBL-*E.coli*.

Better antibacterial activity was obtained for the Nd doped ZnO NP. The authors suggest that this can occur due to its small crystallite size (33 nm) compared to undoped ZnO NP (45 nm). We have found a smaller MIC for ESBL-*E.coli*. compared to that found by Hameed et al., (800 µg/mL) which can be explained by the smaller crystallite size of our ZnO NP (5 nm). In our previous study, we demonstrated that the ZnO NP antibacterial activity was size-dependent when we used standard strains of *S.aureus* and *E. coli* [8]. It has been demonstrated that all the antibacterial mechanisms of ZnO NP were size dependent. This can occur because, with smaller ZnO NP, more particles are needed to cover the bacteria cells and a greater number of ROS is released [45]. A considerable number of studies showed that Zn^{2+} liberation was size dependent [46–48]. Besides, smaller ZnO NP have higher interfacial areas and can easily interact with the bacterial membrane [49]. Thus, ZnO NP with a very small size can result in optimized antimicrobial activity [9].

On the other hand, Ansari et al. used ZnO NP with a size of 19.8 nm to evaluate the antibacterial activity of ZnO NP against ESBL- *E. coli* and *K. pneumoniae*. The authors used 110 clinically isolated samples. The results showed that the MIC values were found to be between 500 and 8000 and the MBC values were between 2000 and 16,000 µg/ml. There were different MIC values that were found. However, 38.1% of ESBL-producing isolates of *E. coli* have an MIC of 1000 µg/ml and 46.3% had an MBC of 4000 µg/ml, while for *K. pneumoniae*, 57.8% have an MIC of 1000 µg/ml and 49.9% have an MBC of 4000 µg/ml [5]. Therefore, even with small ZnO NP sizes, compared to Hameed et al., the highest MIC values were found at higher ZnO NP concentrations. However, the study conducted by Ansari et al. used a lot of clinical isolates and also observed MIC values of 500 µg/ml, albeit in smaller numbers of clinical isolates (22%). Research conducted by Ali et al. [50] used aloe vera extract functionalized with ZnO NP with a size of 350 nm against ESBL-producing clinical isolates of *E. coli*. The MIC value was found to be at 2220 µg/ml, which serves as one more indication that size is an important parameter to optimize antibacterial activity.

Reddy et al. [51] studied the antibacterial activity of ZnO NP against *K. pneumoniae*. The MIC was found to be at 40 µg/ml. With higher concentrations of ZnO NP, there was an increase in the amount of nucleic acids and protein released from the cells. The cytotoxic activities of *K. pneumonia* were evaluated using a human esopharyngeal carcinoma cell line (HEp-2). ZnO NP-treated *K. pneumoniae* were five-fold less infectious for the HEp-2 cell line. Although the MIC values found in our study were higher for *K. pneumoniae*, contrary to Reddy et al., we used a KPC-producing resistant strain. Studies about the MIC of ZnO NP against KPC-*K. pneumoniae* are scarce. However, Misra et al. [52] synthesized iron doped ZnO NP impregnated in kaolinite (ZnO/K) to evaluated their photocatalyst (PCD) disinfection potential against multidrug-resistant *Enterobacter sp*. The strain was resistant to 9 antibiotics, including 6 antibiotic groups (penicillin, carbapenem, cephalosporin, ansamycin, sulfonamide). The results showed that the complete disinfection of *Enterobacter sp* in the water waste was achieved in 120 min by a visible light aided PCD process. The percentage of reduction was not dependent on concentration because, with 150 µg/mL, 7 log reductions have been achieved. On the other hand, with values higher than 150 µg/mL and up to 500 µg/mL, the reduction percentage decreases.

Rojo et al. [53] evaluated clinical characteristics and the profile of resistance associated with KPC- *K. pneumoniae*. The study showed 100% resistance to beta lactams, cephalosporins, and quinolones. Among the carbapenems, 87.25% resistance was found for ertapenem and 56.25% for imipenem. Schmidt-Malan et al. [54] showed high levels of resistance to antimicrobials of KPC- *K. pneumoniae*. Only 5% of KPC-positives were susceptible to imipenem. In addition, only 3 and 2% of KPC-*K. pneumoniae* studied were susceptible to cefepime and ceftriaxone, respectively, and 4% were susceptible to ceftolozano-tazobactam. A recent study performed MIC analyses using the KPC-*K.pneumoniae* isolates with 21 antimicrobial agents, and the isolates showed resistance to most of them [55].

The bactericidal activity was determined to be the lowest concentration at which there was no appearance of colonies when transferred from the liquid medium to the solid. On the other hand, for the bacteriostatic activity, the colonies appear even if there was no growth in the MIC assays [8]. Independent of the strain used, the GPTMS-ZnO NP showed just bactericidal activity at a high concentration of 2500 µg/mL (MBC). Thus, we suggest that GPTMS-ZnO NP had excellent bacteriostatic activity for ESBL-*E. coli* using small nanoparticle concentrations (MIC) - Table 2.

The scarcity of results regarding the use of inorganic nanoparticles against the enterobactericeae family and the results obtained led us to believe that the values obtained for MIC in relation to KPC-*K. pneumoniae* and ESBL-*E. coli*, besides being promising, is an alternative to combat bacterial resistance.

4 Conclusions

The radius of ZnO NP increased throughout the synthesis, more pronouncedly in the beginning of the synthesis (10–20 min) and continued to grow more slowly until 180 min. The GPTMS-ZnO NP had high size stability under different storage conditions, while maintaining their size. The ZnO NP dissolved in acidic pH and were stable at

alkaline pH and produced fractal aggregates at pH 7. Thus, in the current study, we can conclude that the surface modification of ZnO NP allowed the nanoparticles to be dispersed in water, maintaining their size for months. Producing small nanoparticles and ensuring that they remain almost unchanged in size is very important to ensure optimal antibacterial activity. Multiresistant *Enterobacteria* is a global health problem. Studies on ZnO NP activity against multiresistant *Enterobacteria* are scarce, and GPTMS-ZnO NP were not found in the literature, which makes this present study innovative. GPTMS-ZnO NP have great potential to combat multiresistant *Enterobacteria*. However, GPTMS-ZnO NP had had higher bacteriostatic activity against ESBL-producing *Escherichia coli* than KPC-producing *Klebsiella pneumoniae*.

Data availability

All data generated or analyzed during this study are included in this paper. For more details, data supporting the findings of this study are available from the corresponding author on request.

Acknowledgements The authors thank Brazilian Synchrotron light Laboratory (LNLS) for providing beamtime at SAXS1 beamline.

Author contributions The manuscript was written through contributions of all authors. All authors have given approval to the final version of the manuscript.

Funding This work was supported by Fundação de Amparo à Pesquisa do Estado de São Paulo (FAPESP) and Coordenação de Aperfeiçoamento de Pessoal de Nível Superior (CAPES), Finance Code 001.

Compliance with ethical standards

Conflict of interest The authors declare no competing interests.

Publisher's note Springer Nature remains neutral with regard to jurisdictional claims in published maps and institutional affiliations.

References

1. World Health Organization (2016) No time to wait: securing the future from drug-resistant infections. World Heal Organization Geneva, Switzerland
2. Makvandi P, Wang C, Zare EN et al. (2020) Metal-based nanomaterials in biomedical applications: antimicrobial activity and cytotoxicity aspects. Adv Funct Mater. 30:22. https://doi.org/10.1002/adfm.201910021
3. de Oliveira MS, Oshiro-Junior JA, Sato MR et al. (2020) Polymeric nanoparticle associated with ceftriaxone and extract of schinopsis brasiliensis engler against multiresistant enterobacteria. Pharmaceutics 12:695. https://doi.org/10.3390/pharmaceutics12080695
4. Soontaros S, Leelakanok N (2019) Association between carbapenem-resistant Enterobacteriaceae and death: a systematic review and meta-analysis. Am J Infect Control 47:1200–1212. https://doi.org/10.1016/j.ajic.2019.03.020
5. Ansari MA, Khan HM, Khan AA et al. (2012) Synthesis and characterization of the antibacterial potential of ZnO nanoparticles against extended-spectrum β-lactamases-producing escherichia coli and klebsiella pneumoniae isolated from a tertiary care hospital of North India. Appl Microbiol Biotechnol 94:467–477. https://doi.org/10.1007/s00253-011-3733-1
6. Doi Y, Paterson DL(2015) Carbapenemase-Producing Enterobacteriaceae. Semin Respir Crit Care Med 1:74–85
7. Castanheira M, Rhomberg PR, Flamm RK, et al. (2016) Effect of the β-lactamase inhibitor vaborbactam combined with meropenem when tested against serine-carbapenemase-producing enterobacteriaceae. Am Soc fo Microbiol. https://doi.org/10.1128/AAC.00711-16
8. Lallo da Silva B, Caetano BL, Chiari-Andréo BG et al. (2019) Increased antibacterial activity of ZnO nanoparticles: Influence of size and surface modification. Colloids Surf B Biointerfaces 177:440–447
9. Lallo da Silva B, da, Abuçafy MP, Manaia EB et al. (2019) Relationship between structure and antimicrobial activity of zinc oxide nanoparticles: An overview. Int J Nanomed 14:9395–9410. https://doi.org/10.2147/IJN.S216204
10. Raghupathi KR, Koodali RT, Manna AC (2011) Size-dependent bacterial growth inhibition and mechanism of antibacterial activity of zinc oxide nanoparticles. Langmuir 27:4020–4028
11. Janaki AC, Sailatha E, Gunasekaran S (2015) Synthesis, characteristics and antimicrobial activity of ZnO nanoparticles. Spectrochim Acta Part A Mol Biomol Spectrosc 144:17–22
12. Aboulaich A, Tilmaciu CM, Merlin C et al. (2012) Physicochemical properties and cellular toxicity of (poly) aminoalkoxysilanes-functionalized ZnO quantum dots. Nanotechnology. 23. https://doi.org/10.1088/0957-4484/23/33/335101
13. Sharma N, Jandaik S, Kumar S (2016) Synergistic activity of doped zinc oxide nanoparticles with antibiotics: ciprofloxacin, ampicillin, fluconazole and amphotericin B against pathogenic microorganisms. An Acad Bras Cienc 88:1689–1698
14. Pasquet J, Chevalier Y, Couval E et al. (2015) Zinc oxide as a new antimicrobial preservative of topical products: Interactions with common formulation ingredients. Int J Pharm 479:88–95
15. Hameed ASH, Karthikeyan C, Ahamed AP et al. (2016) In vitro antibacterial activity of ZnO and Nd doped ZnO nanoparticles against ESBL producing Escherichia coli and Klebsiella pneumoniae. Sci Rep 6:1–11. https://doi.org/10.1038/srep24312
16. Kumar R, Umar A, Kumar G, Nalwa HS (2017) Antimicrobial properties of ZnO nanomaterials: a review. Ceram Int 43:3940–3961. https://doi.org/10.1016/j.ceramint.2016.12.062
17. Pintaric LM, Skoc MS, Bilic VL et al. (2020) Synthesis, modification and characterization of antimicrobial textile surface containing ZnO nanoparticles. Polymers (Basel) 12:1210
18. Spanhel L, Anderson MA (1991) Semiconductor clusters in the sol-gel process: quantized aggregation, gelation, and crystal growth in concentrated zinc oxide colloids. J Am Chem Soc 113:2826–2833
19. Rissi NC, Hammer P, Chiavacci LA (2017) Surface modification of ZnO quantum dots by organosilanes and oleic acid with enhanced luminescence for potential biological application. Mater Res Express 4:15027
20. Li S, Sun Z, Li R et al. (2015) ZnO nanocomposites modified by hydrophobic and hydrophilic silanes with dramatically enhanced tunable fluorescence and aqueous ultrastability toward biological imaging applications. Sci Rep 5:8475
21. Kohlbrecher J, Bressler I (2014) SAsfit. Paul Scherrer Institut, Villigen, Switzerland

22. Methods for Dilution Antimicrobial Susceptibility Tests for Bacteria that Grow Aerobically. (20th ed.), Clinical and Laboratory Standards Institute, Wayne, PA (2015) M07-A10
23. Asok A, Gandhi MN, Kulkarni AR (2012) Enhanced visible photoluminescence in ZnO quantum dots by promotion of oxygen vacancy formation. Nanoscale 4:4943–4946
24. Tokumoto MS, Pulcinelli SH, Santilli CV, Briois V (2003) Catalysis and temperature dependence on the formation of ZnO nanoparticles and of zinc acetate derivatives prepared by the sol-gel route. J Phys Chem B 107:568–574
25. Guiner A, Fournet G, Walker CB (1955) Small angle scattering of X-rays. J Wiley, Sons, New York, NY
26. Do Kim K, Choi DW, Choa Y-H, Kim HT (2007) Optimization of parameters for the synthesis of zinc oxide nanoparticles by Taguchi robust design method. Colloids Surf A Physicochem Eng Asp 311:170–173
27. Caetano BL, Santilli CV, Meneau F et al. (2011) In situ and simultaneous UV− vis/SAXS and UV− vis/XAFS time-resolved monitoring of ZnO quantum dots formation and growth. J Phys Chem C 115:4404–4412
28. Caetano BL, Briois V, Pulcinelli SH et al. (2016) Revisiting the ZnO Q-dot formation toward an integrated growth model: from coupled time resolved UV–Vis/SAXS/XAS data to multivariate analysis. J Phys Chem C 121:886–895
29. Brus L (1986) Electronic wave functions in semiconductor clusters: experiment and theory. J Phys Chem 90:2555–2560
30. Nedelijkovic JM, Patel RC, Kaufman P et al. (1993) Synthesis and optical properties of quantum-sized metal sulfide particles in aqueous solution. J Chem Educ 70:342
31. Murphy CJ (2002) Peer reviewed: optical sensing with quantum dots Anal Chem 74(19):520 A–526 A
32. Isnaeni, Kim KH, Nguyen DL et al. (2011) Shell layer dependence of photoblinking in CdSe/ZnSe/ZnS quantum dots. Appl Phys Lett 98:1–4. https://doi.org/10.1063/1.3533401
33. Zhang J, Chen J, Yuan Z, Feng J (2018) Zwitterionic coating promotes zinc oxide quantum dot stability and reduces aggregation in biological media. J Nanosci Nanotechnol 18:7713–7720. https://doi.org/10.1166/jnn.2018.15545
34. Li X, Wang G, Li X (2005) Surface modification of nano-SiO 2 particles using polyaniline. Surf Coat Technol 197:56–60
35. Manaia EB, Abuçafy MP, Chiari-Andréo BG et al. (2017) Physicochemical characterization of drug nanocarriers. Int J Nanomed 12:4991
36. Lin P-C, Lin S, Wang PC, Sridhar R (2014) Techniques for physicochemical characterization of nanomaterials. Biotechnol Adv 32:711–726
37. Brinker CJ, Scherer GW (2013) Sol-gel science: the physics and chemistry of sol-gel processing. Academic press. New York
38. Cai X, Luo Y, Yan H et al. (2017) pH-Responsive ZnO Nanocluster for Lung Cancer Chemotherapy. ACS Appl Mater Interfaces 9:5739–5747
39. Liu K-K, Shan C-X, He G-H et al. (2017) Advanced Encryption based on fluorescence quenching of ZnO nanoparticles. J Mater Chem C 5:7167–7173
40. Kumar S, Krishnakumar B, Sobral AJFN, Koh J (2019) Bio-based (chitosan/PVA/ZnO) nanocomposites film: thermally stable and photoluminescence material for removal of organic dye. Carbohydr Polym 205:559–564. https://doi.org/10.1016/j.carbpol.2018.10.108
41. Chen Q, Yakovlev NL (2010) Adsorption and interaction of organosilanes on TiO 2 nanoparticles. Appl Surf Sci 257:1395–1400
42. Leung YH, Chan CMN, Ng AMC et al. (2012) Antibacterial activity of ZnO nanoparticles with a modified surface under ambient illumination. Nanotechnology 23:475703
43. Buşilă M, Tăbăcaru A, Muşsat V et al. (2020) Size-dependent biological activities of fluorescent organosilane-modified zinc oxide nanoparticles. J Biomed Nanotechnol 16:137–152. https://doi.org/10.1166/jbn.2020.2882
44. Farouk A, Moussa S, Ulbricht M et al. (2014) ZnO-modified hybrid polymers as an antibacterial finish for textiles. Text Res J 84:40–51
45. Padmavathy N, Vijayaraghavan R (2016) Enhanced bioactivity of ZnO nanoparticles—an antimicrobial study. Sci Technol Adv Mater 9:035004-035010
46. Wong SWY, Leung PTY, Djurišić AB, Leung KMY (2010) Toxicities of nano zinc oxide to five marine organisms: influences of aggregate size and ion solubility. Anal Bioanal Chem 396:609–618
47. Pasquet J, Chevalier Y, Pelletier J et al. (2014) The contribution of zinc ions to the antimicrobial activity of zinc oxide. Colloids Surf A Physicochem Eng Asp 457:263–274
48. Heinlaan M, Ivask A, Blinova I et al. (2008) Toxicity of nanosized and bulk ZnO, CuO and TiO 2 to bacteria Vibrio fischeri and crustaceans Daphnia magna and Thamnocephalus platyurus. Chemosphere 71:1308–1316
49. Sirelkhatim A, Mahmud S, Seeni A et al. (2015) Review on zinc oxide nanoparticles: antibacterial activity and toxicity mechanism. Nano Micro Lett 7:219–242
50. Ali K, Dwivedi S, Azam A et al. (2016) Aloe vera extract functionalized zinc oxide nanoparticles as nanoantibiotics against multi-drug resistant clinical bacterial isolates. J Colloid Interface Sci 472:145–156. https://doi.org/10.1016/j.jcis.2016.03.021
51. Reddy LS, Nisha MM, Joice M, Shilpa PN (2014) Antimicrobial activity of zinc oxide (ZnO) nanoparticle against Klebsiella pneumoniae. Pharm Biol 52:1388–1397. https://doi.org/10.3109/13880209.2014.893001
52. Misra AJ, Das S, Habeeb Rahman AP et al. (2018) Doped ZnO nanoparticles impregnated on Kaolinite (Clay): A reusable nanocomposite for photocatalytic disinfection of multidrug resistant Enterobacter sp. under visible light. J Colloid Interface Sci 530:610–623. https://doi.org/10.1016/j.jcis.2018.07.020
53. Rojo V, Vázquez P, Reyes S et al. (2018) Risk factors and clinical evolution of carbapenemase-producing klebsiella pneumoniae infections in a university hospital in Spain. Case-control study. Rev Esp Quimioter 31:427–434
54. Schmidt-malan SM, Mishra AJ, Mushtaq A, Brinkman CL (2018) crossm In Vitro Activity of Imipenem-Relebactam and Ceftolozane
55. Zhai Y, Li D, Du P et al. (2020) Complete sequences of two new KPC-harboring plasmids in Klebsiella pneumoniae ST11 strains in China. J Glob Antimicrob Resist. https://doi.org/10.1016/j.jgar.2020.11.023